Available online at www.sciencedirect.com

SciVerse ScienceDirect

Ceramics International 38 (2012) 4751–4760

CERAMICS INTERNATIONAL

www.elsevier.com/locate/ceramint

In situ synthesis of ZrB_2–$MoSi_2$ platelet composites: Reactive hot pressing process, microstructure and mechanical properties

Hai-Tao Liu [a,b], Wen-Wen Wu [a,b], Ji Zou [a,b], De-Wei Ni [a,b], Yan-Mei Kan [a], Guo-Jun Zhang [a,*]

[a] State Key Laboratory of High Performance Ceramics and Superfine Microstructures, Shanghai Institute of Ceramics, Shanghai 200050, China
[b] Graduate School of the Chinese Academy of Sciences, Beijing 100049, China

Received 24 June 2011; received in revised form 14 February 2012; accepted 22 February 2012
Available online 3 March 2012

Abstract

Using elemental Zr, B, Mo and Si as raw materials, partially textured ZrB_2–$MoSi_2$ composites with in situ platelet ZrB_2 grains were fabricated by reactive hot pressing. Synthesized by a combustion reaction, the in situ formed ZrB_2 phase had unique characteristics to grow up to platelet grains, on the surroundings of Mo–Si–B ternary liquid phase at high temperature. Mechanical properties were dependent on grain size and aspect ratio of the ZrB_2 platelets. The rotation and realignment of the platelet ZrB_2 grains under hot pressing led to a partially textured microstructure, which showed anisotropic mechanical properties on different directions of the as-sintered samples. A roadmap of the reaction process, microstructure evolution and texture formation was given to describe the preparation of partially textured ZrB_2–$MoSi_2$ composites by reactive hot pressing.

Keywords: B. Platelets; C. Mechanical properties; E. Structural applications; Reactive hot pressing

1. Introduction

ZrB_2-based composite ceramics, as a kind of typical ultra high-temperature ceramics (UHTCs), has attracted much attention in recent years [1]. Although ZrB_2 has a unique combination of excellent properties, yet densification and poor oxidation resistance are major shortcomings which hinder its actual applications [2,3]. Besides, poor thermal shock resistance is another disadvantage which becomes more salient nowadays [4,5]. Combining another phase, such as SiC [6–9] and $MoSi_2$ [10], ZrB_2-based composite ceramics can be obtained. In ZrB_2-based composite ceramics, not only the above shortcomings can be overcome, but also some performances of the composites can be improved because of the excellent properties of the second phase itself, which make ZrB_2-based composites suitable for practical and potential applications for the hypersonic aerospace vehicles and re-usable atmospheric re-entry vehicles [11,12].

ZrB_2–$MoSi_2$ composite is an important kind of ZrB_2-based UHTCs [10,13,14]. $MoSi_2$, another kind of refractory ceramics, is widely used as elevated-temperature structural material owing to its moderate density of 6.24 g/cm^3, a high melting point (2030 °C) and excellent oxidation resistance [15,16]. When using $MoSi_2$ as a second phase to prepare ZrB_2-based ceramics, densified composite can be obtained at a lower temperature (1750–1850 °C [17–19]) compared to monolithic ZrB_2 ceramics (2100–2300 °C [10]), due to the plastic character of $MoSi_2$ which makes it fill the voids of ZrB_2 skeleton to form a pore-free structure. Besides, the oxidation resistance of ZrB_2-based composites can also be improved by the help of the $MoSi_2$.

ZrB_2–$MoSi_2$ composite can be obtained by different densification techniques. Sciti et al. have prepared ZrB_2–$MoSi_2$ composites by pressureless sintering (PLS) [13,17,20], hot pressing (HP) [14,17] and spark plasma sintering (SPS) [14,17,21]. On the other hand, Wu et al. used the method of reactive hot pressing (RHP) [18]. It should be noted that when using RHP, ZrB_2–$MoSi_2$ composites with in situ elongated ZrB_2 grains can be obtained, whose microstructure was different from those prepared by non-reactive process (PLS, HP and SPS) and the mechanical properties could be improved.

* Corresponding author. Tel.: +86 21 52411080; fax: +86 21 52413122.
E-mail address: gjzhang@mail.sic.ac.cn (G.-J. Zhang).

0272-8842/$36.00
doi:10.1016/j.ceramint.2012.02.061

Table 1
Thermodynamic data of the reactions.

$Zr + 2B + xMo + 2xSi = ZrB_2 + xMoSi_2$	Enthalpy ΔH^o_{298} (kJ)	Free energy ΔG^o_{298} (kJ)	Free energy ΔG^o_{2073} (kJ)	$\Delta H^o_{298}/C_{p298}$ (K)	Adiabatic temperature T_{ad} (K)[a]
$x = 0.0845$ (ZM10)	−332.627	−328.115	−285.034	6200	3954
$x = 0.1900$ (ZM20)	−345.163	−340.614	−294.542	5714	3767
$x = 0.3258$ (ZM30)	−361.300	−356.703	−306.781	5229	3569

[a] The melting enthalpies of ZrB_2 and $MoSi_2$ were not considered in the calculation.

Furthermore, in situ platelet-reinforced and textured ZrB_2-based ultra high temperature ceramics are prepared by Liu et al. via RHP and successive hot-forging (HF), and the flexural strength after hot-forging have been improved by 52% compared with that before hot-forging, indicating that the platelet ZrB_2 grains is beneficial for the properties of the composites [22]. In situ synthesis is a regular method to prepare boride composites [23,24], and the appearance of in situ formed platelet ZrB_2 grains in the ZrB_2-based composites is an interesting phenomenon.

Up to now, the growth mechanism of the platelet ZrB_2 grains in the RHPed ceramics is still not clear. Besides, the relationship between the mechanical properties and the microstructure, especially the effect of the aspect ratio of the ZrB_2 platelet grains, also need further investigation. So in the present paper, the reaction process of the Zr–B–Mo–Si system was investigated to make clear the mechanism of the platelet grains growth. The mechanical properties of the obtained partially textured composites with different amounts of $MoSi_2$ and holding time were studied. Meanwhile, properties on different surfaces of the samples were also discussed.

2. Thermodynamic consideration

The ZrB_2–$MoSi_2$ composites fabricated by reactive hot pressing using elemental Zr, B, Mo and Si in the present study were based on the following reaction:

$$Zr + 2B + xMo + 2xSi \rightarrow ZrB_2 + xMoSi_2 \quad (1)$$

where $x = 0.0845$, 0.1900 and 0.3258 for ZM10, ZM20 and ZM30 (short for ZrB_2 with 10, 20 and 30 vol.% $MoSi_2$ composites), respectively. A commercial software package (HSC Chemistry 6.1 Outokumpu Research Oy, Pori, Finland) was used for the thermodynamic analysis. The data of the free energy changes with the temperature in the reactions are listed in Table 1. It can be seen that all the three reactions are highly exothermic and thermodynamically favorable. Besides, they all satisfy the thermodynamic conditions for self-sustaining combustion process ($T_{ad} \geq 1800$ K and $\Delta H^o_{298}/C_{p298} > 2000$ K) [25,26]. It means that these composites could be produced by self-propagating high-temperature synthesis (SHS) or simultaneous combustion synthesis (CS) based on the thermodynamic consideration.

3. Experimental procedure

Commercial powders of Zr (purity > 98%, particle size < 28 μm), amorphous B (purity > 96%, particle size < 1 μm), Mo (purity > 99%, particle size < 74 μm) and Si (purity > 99%, particle size < 50 μm) were used as starting materials. Three different stoichiometric powders were prepared, which were ZM10, ZM20 and ZM30 (Table 1). They were mixed by planetary ball milling in acetone at 560 rpm for 8 h using ZrO_2 balls as milling media. After milling, the powders were dried in a rotary evaporator at 70 °C and then sieved through a 200-mesh screen. The as-treated powder mixtures were placed in a graphite die (37 mm × 30 mm) with a BN coating. The mixtures in the graphite die were applied with a pressure of 10 MPa for 5 min at room temperature and then were RHPed at a heating rate of 10 °C/min at a vacuum level of <10 Pa. The furnace was heated to about 1550 °C and held at this temperature for 30 min; then a pressure of 20 MPa was applied and the furnace was backfilled with argon gas. Subsequently the samples were heated to the final temperature with different holding time (1 h for ZM10 and ZM30; and 0.5, 1 and 2 h for ZM20, as shown in Table 2). The increase of temperature, the change of vacuum level inside the furnace and the pressure applied were fully monitored and recorded in the processing.

The bulk densities of RHPed samples were measured by Archimedes technique after removing the outer layer by grinding, using distilled water as immersing medium. Examination of phase composition was carried out via X-ray diffractometry (D/max 2250V, Rigaku, Tokyo, Japan) using CuKα radiation. The microstructure of the samples was analyzed using scanning electron microscopy (Hitachi S-570,

Table 2
Components and densities of the samples.

Sample no.	Components	Sintering temperature and time	Density (g/cm^3)	Relative density (%)
ZM10-1 h	ZrB_2–10 vol%$MoSi_2$	1800 °C/1 h	6.101	99.9
ZM30-1 h	ZrB_2–30 vol%$MoSi_2$	1800 °C/1 h	6.119	99.7
ZM20-0.5 h	ZrB_2–20 vol%$MoSi_2$	1800 °C/0.5 h	6.110	99.8
ZM20-1 h	ZrB_2–20 vol%$MoSi_2$	1800 °C/1 h	6.114	99.9
ZM20-2 h	ZrB_2–20 vol%$MoSi_2$	1800 °C/2 h	6.115	99.9

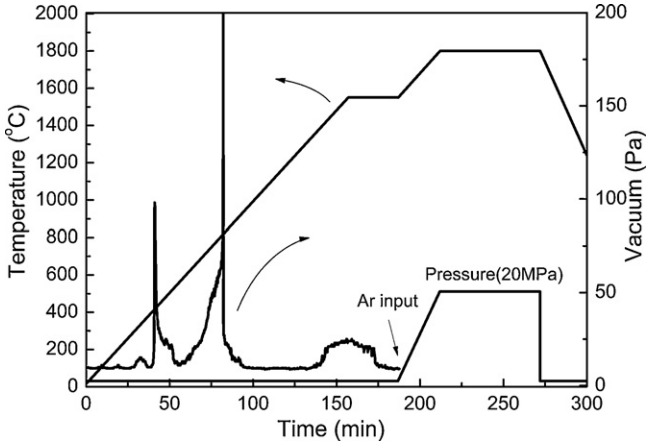

Fig. 1. Reactive hot pressing program with the change of vacuum level.

Tokyo, Japan) and transmission electron microscopy (JEM 2100F, Tokyo, Japan). Three-point bending strength was measured on bars with dimensions of 2 mm × 2.5 mm × 30 mm using a span of 20 mm and a crosshead speed of 0.5 mm min^{-1}. Vickers hardness and fracture toughness were tested by the indentation technique on polished samples. Indentations were made using a 10 kg load with a dwell of 10 s. According to the indentation crack lengths, the fracture toughness was calculated.

4. Results and discussion

4.1. Reaction process

The changes of the vacuum level in the furnace with the increasing temperature are shown in Fig. 1. The vacuum level was maintained below 10 Pa during the beginning of the sintering process. With the increase of the temperature, there were two vacuum level "peaks" in the heating process. The first lower "peak" (~100 Pa at most) was at about 500 °C and the second higher "peak" (>200 Pa and exceeding the measuring range of vacuometer) was in the temperature range from 800 to 1000 °C.

XRD patterns of the raw materials, the powders at 500 °C and 1000 °C are shown in Fig. 2. It can be seen that at 400–500 °C (Fig. 2(b)), the components of the samples were partially the same with the raw materials, but there were some other components, especially the transition phase of ZrH_x (x = 1 or 2), appearing at this temperature with the decline of the vacuum level. It was hypothesized that there were some chemical reactions except reaction (1) occurred at this temperature, such as:

$$3Zr + 2H_2O(g) = 2ZrH_2 + ZrO_2 \quad (2)$$

$$5Zr + 2H_2O(g) = 4ZrH + ZrO_2 \quad (3)$$

$$ZrH_2 = Zr + H_2(g) \quad (4)$$

$$2ZrH = 2Zr + H_2(g) \quad (5)$$

The free energy (ΔG) of reactions (2) and (3) are negative, while (4) and (5) are positive at this temperature range. H_2O was from the air moisture by absorbing on the surface of the starting powders.

When temperature reached to 800–1000 °C, there was a sharp vacuum level "peak", meaning that there was an acute decline of the vacuum level. XRD patterns (Fig. 2(c)) shows that the components at 1000 °C were crystalline phases of ZrB_2 and $MoSi_2$. The thermodynamic calculations discussed above have showed that the reaction satisfies the thermodynamic conditions for self-sustaining combustion process. So it could be deduced that there was a combustion reaction among the raw materials and gas emitting appeared simultaneously, which led to the sharp decline of vacuum level. Besides, the violent exothermic reaction could generate a great deal of heat, which could volatilize low boiling point impurities [25]. As a result, purely ZrB_2 and $MoSi_2$ could be obtained according to the XRD patterns analysis. The possible reactions occurred in this process could be shown as follows:

$$Zr + 2B + xMo + 2xSi = ZrB_2 + xMoSi_2 \quad (1')$$

$$ZrH_2 = Zr + H_2(g) \quad (4')$$

$$2ZrH = 2Zr + H_2(g) \quad (5')$$

$$1.5ZrO_2 + 5B = 1.5ZrB_2 + B_2O_3(g) \quad (6)$$

$$Si + SiO_2 = 2SiO(g) \quad (7)$$

Among these reactions, free energies (ΔG) of (1′), (4′) and (5′) are negative in this temperature range when the vacuum level is about 10 Pa, but those of (6) and (7) are positive; the required energy (ΔH) of reactions (4), (5), (6) and (7) can be compensated by the heat released in the reaction (1).

As the end phases of ZrB_2 and $MoSi_2$ were synthesized at 1000 °C, densification of the ZrB_2–$MoSi_2$ composites should be the main process in the following heating procedure. Table 2 shows that all the samples are dense when sintered at 1800 °C.

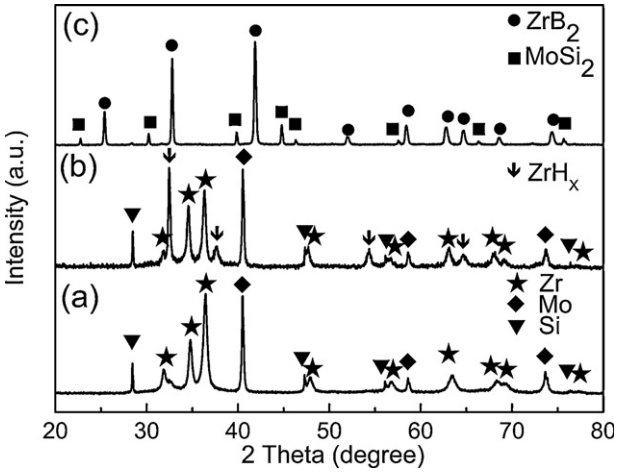

Fig. 2. XRD patterns of (a) raw materials (Zr, amorphous B, Mo and Si), (b) powders after heat treated 500 °C and (c) powders after combustion at 1000 °C. At 500 °C, there existed ZrH_x phase; while at 1000 °C, there were only the end phases of ZrB_2 and $MoSi_2$.

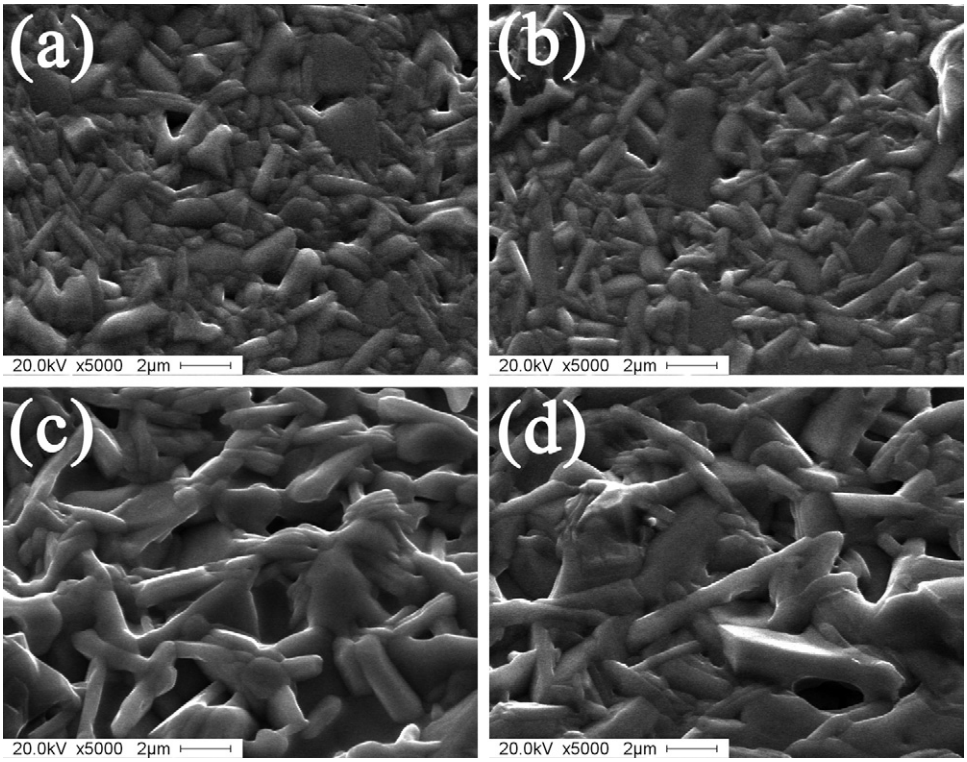

Fig. 3. SEM images of surfaces of the as-sintered samples after polishing and thermal etching: (a) ZM10-1 h, (b) ZM20-1 h, (c) ZM30-1 h and (d) ZM20-2 h.

It is known that the reactive sintering contains three types: reaction before sintering, sintering before reaction and simultaneous reaction and sintering. In the present study, the process is obviously the type of reaction before sintering. Owing to the reaction, powders synthesized in the combustion process had highly chemical reactivity which was beneficial for the densification of the samples.

4.2. Mechanism of anisotropic growth

The as-sintered samples with different contents of $MoSi_2$ and different holding times are shown in Fig. 3, where lots of platelet ZrB_2 grains interlocking to each other can be seen.

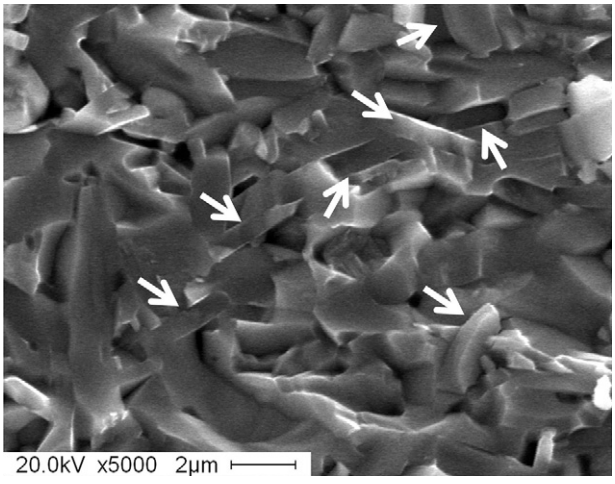

Fig. 4. SEM image of the fracture surface of the sample ZM30-1 h. The arrows show the pulled out platelet grains.

Fracture surface of ZM30-1 h is shown in Fig. 4. The intergranular fracture mode was different from those samples prepared by PLS, HP and SPS [17] which showed transgranular fracture. It is suggested that the coarse fracture surface is attributed to the platelet grains pulled-out in the fracture surface in the RHP samples (the arrows in Fig. 4).

Most of the ZrB_2 grains are developed to platelet morphology when using elemental Zr, B, Mo and Si as raw material and prepared by RHP, while ZrB_2 platelet grains were not found in the hot pressed ZrB_2–$MoSi_2$ composites when using ZrB_2 and $MoSi_2$ as raw materials [10,17]. So it is the reactive hot pressing which presents anisotropic growth of ZrB_2 grains in the ZrB_2–$MoSi_2$ system. Additionally, we have proved that the anisotropic growth is independent of the hot pressing, because platelet ZrB_2 grains can also form in the reactive sintering process when no pressure was applied. Therefore, the reactive process in the present experiment is essential for the anisotropic growth of the ZrB_2 grains.

As discussed in Section 4.1, some elemental Zr formed ZrH_x at about 500 °C, so ZrH_x is one reactant in the combustion process at 800–1000 °C. Zhang et al. once used TiH_2 as one of raw materials to produce TiB_2-based composites by reactive hot pressing [27–29], and the products had platelet TiB_2 grains. Similarly, it was hypothesized that the transient ZrH_x phase as reactant appeared in the present study is beneficial for the anisotropic growth of ZrB_2 grains to form platelet morphology. Detail mechanisms of the anisotropic growth of ZrB_2 grains should be explored in the future investigation. Recently, Ran et al. also obtained partially textured TiB_2–SiC composites by reactive pulsed electric current sintering of attrition-milled TiH_2–B–SiC–B_4C powder mixtures [30].

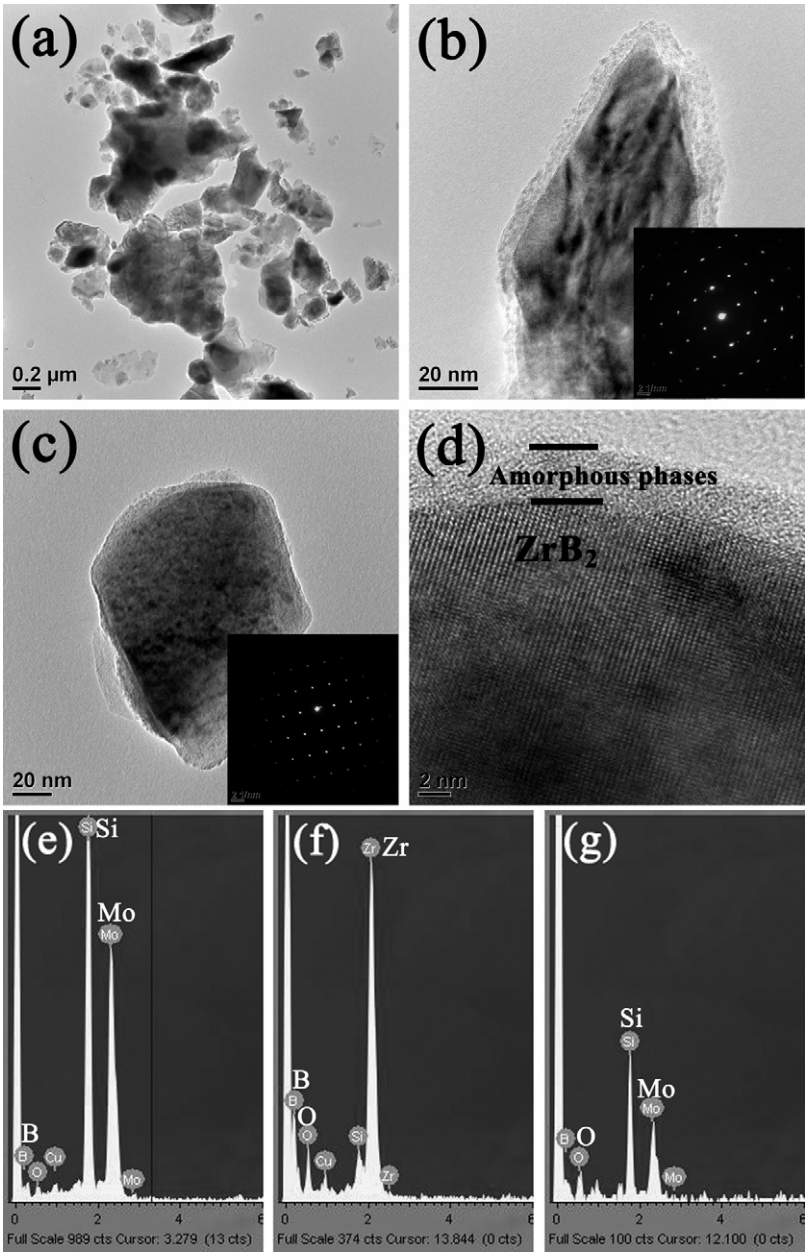

Fig. 5. TEM images of ZrB_2 and $MoSi_2$ mixed powders after combustion reaction at 1000 °C: (a) a general view, (b) $MoSi_2$ particle with its electronic diffraction pattern, (c) ZrB_2 particle with its electronic diffraction pattern and (d) HRTEM of ZrB_2 particle in (c). (e–g) EDS spectra images of ternary Mo–Si–B, Zr–B–O and Mo–Si–O particles, respectively.

Besides, different from the commercial ZrB_2 powders, the ZrB_2 and $MoSi_2$ powders formed at 1000 °C after the combustion reaction must have unique advantages, which lead them to form platelet grains. TEM images of the ZrB_2 and $MoSi_2$ powders after combustion reaction are shown in Fig. 5(a)–(c). The powders were partially agglomerated from fine primary particles. It can be seen that the particle size is less than 600 nm, which is much smaller than that of commercial powders (about 1–5 μm). In addition, HRTEM images of ZrB_2 (Fig. 5(d)) showed that at the rim of the particles, there were some amorphous phases which enclosed the grain surface, and the same ''core-rim'' structure also existed in $MoSi_2$ phase. On the other hand, EDS analysis also showed that there were some amorphous phase (particles) of Mo–Si–B, as well as a small amount of Zr–B–O and Mo–Si–O (Fig. 5(e)–(g)). Silvestroni et al. once revealed that the Mo–Si–B phase were liquid at high temperature, which could promote the densification of the composite [31]. It is known that ZrB_2 belongs to hexagonal system, and the surface energy on the (0 0 1) planes is higher than other planes, such as (1 0 0) and (1 1 0), so the low activation energy diffusion paths are along <2 1 0> and <1 0 0> direction, respectively [32]. In fact, however, there are seldom platelet ZrB_2 grains in the ceramics which are prepared using commercial ZrB_2 and $MoSi_2$ powders. In our experiment, the ZrB_2 grains in the powders at 1000 °C are still globular, but in the final product, the ZrB_2 grains are platelet. Therefore, it can be concluded that the in situ formed liquid phase imposed the catalysis effect on the growth of ZrB_2 grains. With the

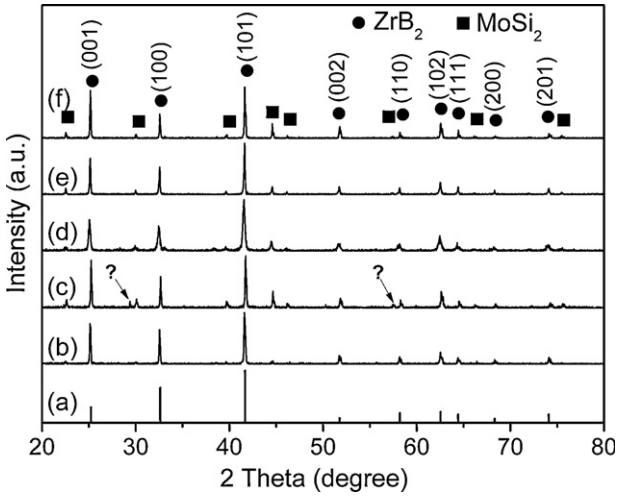

Fig. 6. XRD patterns of the samples: (a) standard JCPDS card (34-0423), (b) ZM10-1 h, (c) ZM30-1 h, (d) ZM20-0.5 h, (e) ZM20-1 h and (f) ZM20-2 h.

increase of the temperature, the liquid phase can wet the grain boundary, and the Zr and B atoms in the liquid phase will easily transport to the low surface energy planes ((1 0 0) or (1 1 0) planes) of ZrB_2 grains, which favors in the elongation of ZrB_2 grains along the *a*- and *b*-axis resulting from the Ostwald ripening at higher temperature.

4.3. Partially textured microstructure

Hot pressing was one of the useful methods for preparing textured structural ceramics [33]. In the present study, partially textured ZrB_2–$MoSi_2$ composites with in situ formed platelet ZrB_2 grains were obtained during the hot pressing process. XRD patterns of the sample surfaces vertical to the hot pressing direction with different amounts of $MoSi_2$ (from 10 to 30 vol.%) and different holding time at 1800 °C (from 0.5 to 2 h) of 20 vol.% $MoSi_2$ are shown in Fig. 6. It could be seen that the (0 0 1) peaks on the surface vertical to the hot pressing direction of all samples became stronger, compared with that of the standard JCPDS card. Here the Lotgering orientation factor, $f(0\,0\,l)$, was used to evaluate the degree of orientation, according to the following equations [34]:

$$f = \frac{P - P_0}{1 - P_0}$$

$$P \text{ and } P_0 = \frac{\sum I_{(00l)}}{\sum I_{(hkl)}}$$

where $\sum I_{(0\,0\,l)}$ and $\sum I_{(h\,k\,l)}$ are the sums of the diffraction peak intensities of the (0 0 *l*) and (*h k l*) planes, respectively. The *P* values were calculated from the measured XRD data on the surface vertical to the hot pressing direction of the samples, while the P_0 values were calculated from the standard JCPDS card (34-0423) of ZrB_2. Based on the XRD intensity data collected, the Lotgering orientation factor $f(0\,0\,l)$ of samples with different contents of $MoSi_2$ and different holding time were obtained. The $f(0\,0\,l)$ of ZM10-1 h, ZM20-1 h and ZM30-1 h were 0.32, 0.33 and 0.35, respectively. While the $f(0\,0\,l)$ of the samples of ZM20-0.5 h, ZM20-1 h and ZM20-2 h were 0.28, 0.33 and 0.38, respectively. Obviously, with the increase of the amount of $MoSi_2$, the Lotgering orientation factor $f(0\,0\,l)$ was increasing. Meanwhile, increasing the holding time could also increase the Lotgering orientation factor $f(0\,0\,l)$.

When the amount of $MoSi_2$ was increasing, there would be more Mo–Si–B ternary compound and $MoSi_2$ phase in the composites: the former would be suitable for the anisotropic growth of the ZrB_2 grains to form platelet morphology, and the latter was ductile at high temperature which could help the platelet grains to rotate and realign perpendicular to the hot pressing direction. It has proved that the ZrB_2 grains grow along *a*- and *b*-axis to form platelet morphology. So when the platelet grains aligned normal to the hot pressing direction, the (0 0 *l*) peaks of ZrB_2 on the surface vertical to the hot pressing direction would surely become stronger. Similarly, when prolonging the holding time at the sintering temperature for the composites with the same amount of $MoSi_2$ (20 vol.%), the Lotgering orientation factor $f(0\,0\,l)$ would also be increased. It was because that a longer holding time could supply more chances for the ZrB_2 platelet grain to grow and realign, resulting in a higher orientation factor.

4.4. Roadmap of ZrB_2–$MoSi_2$ composites by reactive hot pressing

Above all, a schematic illustration of the reaction process and the microstructure development are shown in Fig. 7. The raw materials: elemental B, Mo and Si were in several micrometers, while the elemental Zr was in about 20–30 μm (Fig. 7(a)). When the temperature reached to 400 °C (Fig. 7(b)), small amounts of the raw materials began to react to form several transient phases, such as ZrH_x. At around 900 °C (Fig. 7(c)), a combustion reaction occurred acutely; and at this stage the above transient phases and the raw materials reacted and formed the end phases of ZrB_2 and $MoSi_2$, with the eliminating of the impurities which were existed in the raw materials or introduced in the powder preparation process. The as-formed ZrB_2 and $MoSi_2$ grains were less than 600 nm, indicating a large surface energy, which had high sinterability and the unique characteristics for the formation of anisotropic platelet morphology. Besides, there also existed some other phases, such as the Mo–Si–B ternary phase, which melted at high temperature, might have helped the formation process of the ZrB_2 platelet grains (Fig. 7(d)). At high temperature, when the ZrB_2 platelets grew larger, the platelet ZrB_2 grains would rotate and realign under the uniaxial hot pressure to form a partially textured microstructure. At this stage it is believed that the ductility of $MoSi_2$ (Fig. 7(e)) attributed to the rotation and realignment process of ZrB_2 platelets. The unique microstructure in the ZrB_2–$MoSi_2$ composites by reactive hot pressing could be explained as a combination of the following aspects:

(1) The ZrB_2 and $MoSi_2$ particles by the synthesis of combustion reaction were small (<600 nm) and reactive. The in situ formed fresh powders had a unique ability to grow anisotropic ZrB_2 platelets.

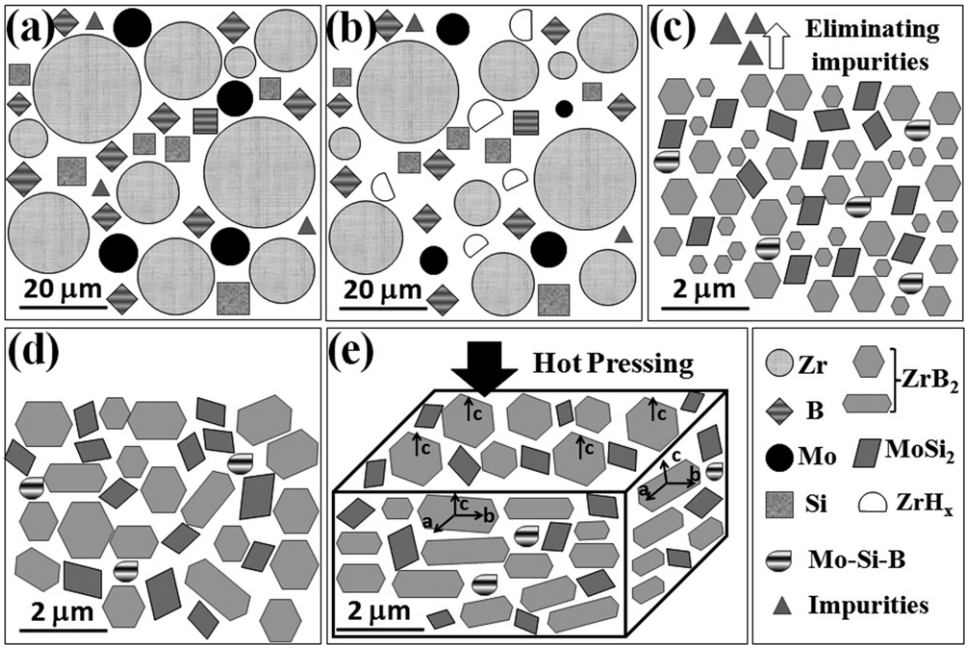

Fig. 7. Roadmap of the preparation of ZrB_2–$MoSi_2$ composites with ZrB_2 platelet grains by reactive hot pressing.

(2) The ternary phases of Mo–Si–B, Zr–B–O and Mo–Si–O formed in the combustion reaction process covered the new formed small ZrB_2 grains and assisted the anisotropic growth of the ZrB_2 grains, because the ternary phases were in their liquid state at high temperature.
(3) The $MoSi_2$ phase exhibited plasticity at temperatures above the brittle–ductile transition temperature (~1000 °C), which has a positive effect on the rotation and arrangement of the ZrB_2 platelet grains.
(4) Hot pressing was also necessary for the rotation and arrangement of the ZrB_2 platelet grains and the formation of the partially textured microstructure.

4.5. Mechanical properties

As there were platelet ZrB_2 grains appearing in the composites by RHP, the relationship between the unique microstructure and their mechanical properties is interesting to be investigated. The mechanical properties of the ZrB_2–$MoSi_2$ composites with different $MoSi_2$ contents and different holding time, as well as properties on different surfaces of the composites were investigated.

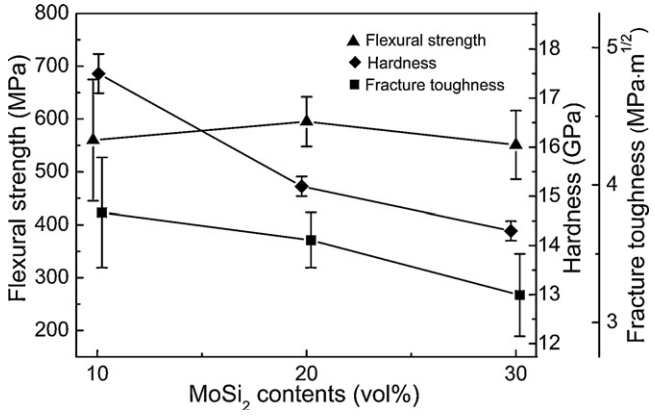

Fig. 8. Mechanical properties of ZrB_2–$MoSi_2$ composites with different content of $MoSi_2$.

4.5.1. Effect of $MoSi_2$ contents

The mechanical properties including 3-point flexural strength, Vicker's hardness and fracture toughness, are shown in Fig. 8, when adding different amounts of $MoSi_2$ into the composites and holding for the same time (1 h) at the sintering temperature. The flexural strength seems to be independent on the content of $MoSi_2$ from 10 to 30 vol.%. While increasing the contents of $MoSi_2$, the hardness and fracture toughness were decreasing, especially the hardness.

SEM images showed that all the three samples have microstructures with anisotropically grown ZrB_2 platelet grains (Figs. 3(a)–(c) and 4). It could be concluded that the ZrB_2 platelet grains could form in a wide range of the amount of $MoSi_2$, at least from 10 to 30 vol.% based on the current study. Moreover, when the content of $MoSi_2$ reached 30 vol.%, the platelet ZrB_2 grains grew much larger than those of 10 and 20 vol.% $MoSi_2$. The aspect ratios of the ZM10, 20 and 30 were 4.3, 4.6 and 5.4, respectively. Although there is a little difference in flexural strength values (551–595 MPa) for the three specimens with different $MoSi_2$ contents, the flexural strengths are considered to be similar. The flexural strength of $MoSi_2$ (~250 MPa [15] was not as good as ZrB_2 (489–493 MPa [1]), and more $MoSi_2$ would have a negative effect on the strength of the composites. On the other hand, ZrB_2 platelets with a suitable grain size and aspect ratio would be beneficial to the material strength, which can compensate the decrease of the flexural strength with more $MoSi_2$ phase. Besides, with increasing the amount of $MoSi_2$, the hardness and fracture toughness of the samples were both decreasing, which could be

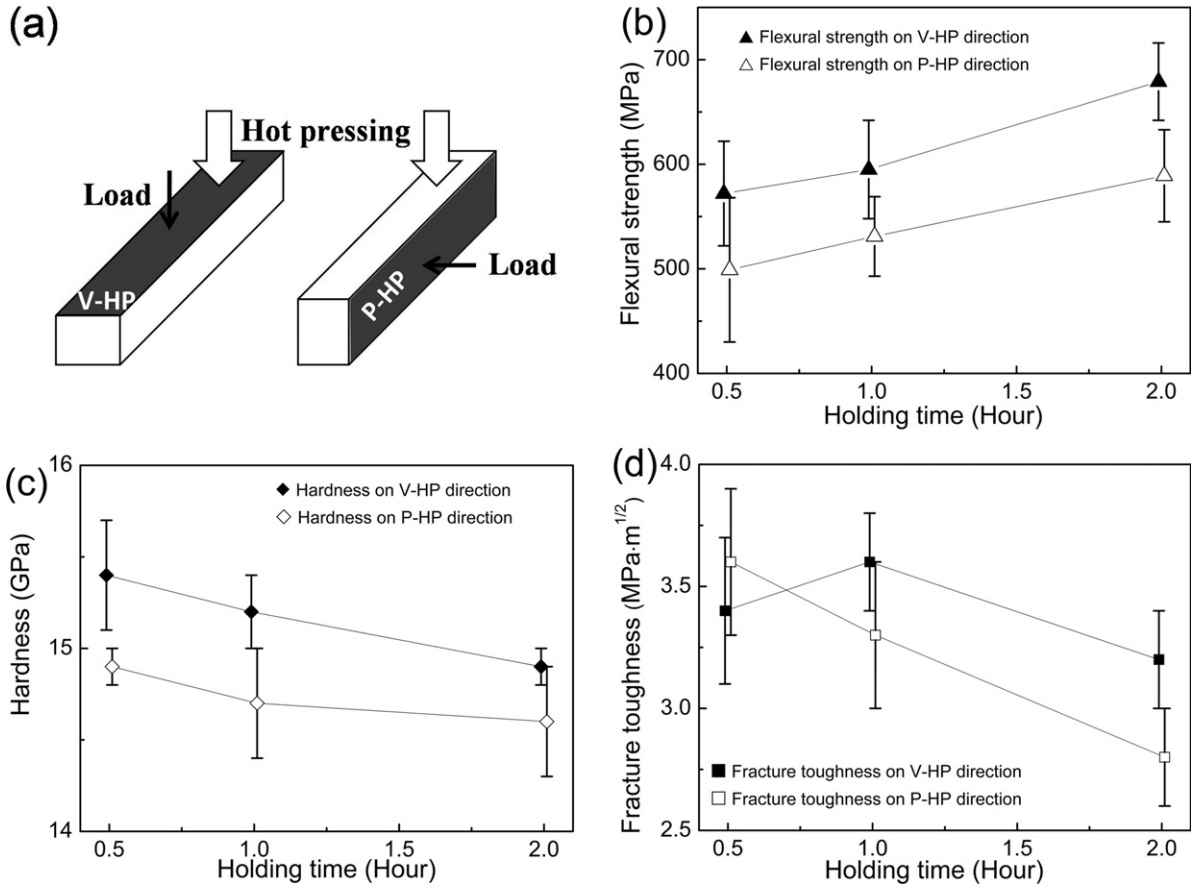

Fig. 9. Mechanical properties of the ZrB_2–20 vol.%$MoSi_2$ composites with different holding time: (a) relationships of the loading direction and the hot pressing direction and (b–d) flexural strength, hardness and fracture toughness, respectively.

explained that the hardness and fracture toughness were much dependent on the intrinsic properties of the phases of ZrB_2 and $MoSi_2$. $MoSi_2$ had a lower hardness (8–10 GPa [15]) and fracture toughness (2.5–3 MPa $m^{1/2}$ [15]) than ZrB_2 (21–23 GPa and 3.5–4.2 MPa $m^{1/2}$, respectively [1]), so the more $MoSi_2$ was added, the lower the composites' hardness and toughness. Therefore, it could be deduced that proper content of $MoSi_2$ was crucial to obtain a composite with optimized properties.

4.5.2. Effect of holding time

Holding time is another factor which has an effect on the aspect ratio of the ZrB_2 platelets. In the present study, ZrB_2–20 vol.%$MoSi_2$ composites were prepared with different holding time. The microstructures of the composites are also shown in Fig. 3(b) and (d) and the mechanical properties are shown in Fig. 9. When prolonging the holding time at 1800 °C, the flexural strength was increasing in direct proportion to the holding time, while the changes of hardness and fracture toughness were opposite.

SEM images showed that the ZrB_2 platelet grains grew larger with prolonging the holding time (Fig. 3(b) and (d)) and the aspect ratio of the platelet grains also became larger. For ZrB_2–20 vol.%$MoSi_2$ composites, a rough estimate based on the SEM images showed that the grain size is about 1.8, 2.9 and 4.6 μm when the holding time is 0.5, 1 and 2 h, respectively. So it can be considered that the grains size has a positive effect on the flexural strength of the composites. A larger grain size leads to a higher strength. Besides, the aspect ratios of the composites holding for 0.5, 1 and 2 h were 3.9, 4.6 and 5.0, respectively. So the aspect ratio is another factor which is beneficial for the strength. Owing to the larger difference in the grain size than the aspect ratio, it is considered that the grain size plays a more important role on the flexural strength.

4.5.3. Mechanical properties on different directions

Fig. 9 also shows the contrast of mechanical properties of two different directions in each sample, which were V-HP and P-HP directions short for the directions vertical and parallel to the hot pressing direction, respectively. It was clear that either the flexural strength or the Vickers hardness on the V-HP direction was superior to those on the P-HP direction in all the samples of ZM20-0.5, 1 and 2 h.

The differences in mechanical properties should also be attributed to the partially textured microstructure with platelet ZrB_2 grains. The differences in mechanical properties should be attributed to the platelet ZrB_2 grains and the partially textured microstructure. Although the degree of orientation is not very high, yet the platelet ZrB_2 grains can still arrange to some extent. Moreover, as shown in Fig. 7, more (0 0 *l*) planes of the platelet grains will overlap to each other under the pressure, resulting in more (0 0 *l*) planes on the V-HP direction and more (*h k* 0) planes on the P-HP direction. Therefore, when the load

is vertical to the V-HP direction surface, the overlapped platelet grains will counteract the load and delay the crack propagation. The cleavage of the plane will consume more energy of the external load, so the strength will be improved on the V-HP direction. When the load is applied on the P-HP surface, however, the direction of the load is parallel to the (0 0 *l*) planes, so the counteraction of the overlapped platelet will not work for the strength, resulting in a relative low flexural strength. Besides, The coefficients of thermal expansion (CTE) of the ZrB_2 grain is anisotropic with $\alpha_a = 5.61 \times 10^{-6}\,K^{-1}$ and $\alpha_c = 6.74 \times 10^{-6}\,K^{-1}$ [35], whereas that of $MoSi_2$ is $\alpha = 9 \times 10^{-6}\,K^{-1}$ [36]. The CTE of ZrB_2 along the *c*-axis is greater than that along the *a*-axis and more close to that of $MoSi_2$. Therefore, on the V-HP direction of the sample, with more planes vertical to the *c*-axis, there exists a weak normal tensile stress in the ZrB_2 platelet grains, leading to a stronger interfacial bonding. However, on the P-HP direction with more planes parallel to the *c*-axis, a large normal tensile stress would exist owing to a large mismatch between α_a of ZrB_2 and α of $MoSi_2$. Wen et al. considered that the interfacial stress attracts cracks, rendering the cracks propagate tortuously along the interfaces, and therefore consume more fracture energy and produce toughening effects [37]. So the weak normal tensile stress on the V-HP direction should be beneficial for the mechanical properties when the load is applied. While the status on the P-HP direction is just the opposite, leading to a relatively lower mechanical properties.

Compared with those of ZrB_2–$MoSi_2$ composites prepared by other methods [17], the fracture toughness of ZrB_2–$MoSi_2$ composites by RHP have been improved owing to the partially texture structure with in situ platelet ZrB_2 grains. Higher fracture toughness is propitious to the thermal shock resistance; therefore, the addition of $MoSi_2$ to the ZrB_2-base composites can not only improve the oxidation resistance, but also enhance the thermal shock resistance of the composites. Furthermore, the brittleness of $MoSi_2$ can be overcome by the assistance of the in situ formed platelet ZrB_2 grains. All of the above discussed show that ZrB_2–$MoSi_2$ composites have integrative performances that combine multitudinous excellent properties.

5. Summary

Partially textured ZrB_2–$MoSi_2$ composites with platelet ZrB_2 grains by reactive hot pressing, using elemental Zr, B, Mo and Si as raw materials, were investigated. Reaction process and mechanism of anisotropic growth of ZrB_2 platelet grains were studied. The in situ formed ZrB_2 particles have small grain sizes and high chemical reactivity, and the Mo–Si–B liquid phase formed in the combustion reaction is beneficial for anisotropic growth of fine ZrB_2 grains. The grain size and aspect ratio of the ZrB_2 platelets have positive effects on the mechanical properties of the as-sintered samples. Hot pressing could make the ZrB_2 platelet grains to rotate and realign to form a partially textured microstructure by the help of the plastic $MoSi_2$ at high temperature. A roadmap of the reaction process and textured microstructure formation were given to interpret the entire route of the reactive hot pressed ZrB_2–$MoSi_2$ composites. Textured ZrB_2-based composites with anisotropic properties would provide an opportunity for the material design and applications of the family of the UHTCs.

Acknowledgements

Financial support from the Chinese Academy of Sciences under the Program for Recruiting Outstanding Overseas Chinese (Hundred Talents Program), the National Natural Science Foundation of China (Nos. 50632070 and 91026008), and the CAS Special Grant for Postgraduate Research, Innovation and Practice are greatly appreciated.

References

[1] W.G. Fahrenholtz, G.E. Hilmas, I.G. Talmy, J.A. Zaykoski, Refractory diborides of zirconium and hafnium, J. Am. Ceram. Soc. 90 (2007) 1347–1364.
[2] S.R. Levine, E.J. Opila, M.C. Halbig, J.D. Kiser, M. Singh, J.A. Salem, Evaluation of ultra-high temperature ceramics for aeropropulsion use, J. Eur. Ceram. Soc. 22 (2002) 2757–2767.
[3] S.Q. Guo, Densification of ZrB_2-based composites and their mechanical and physical properties: a review, J. Eur. Ceram. Soc. 29 (2009) 995–1011.
[4] F. Monteverde, L. Scatteia, Resistance to thermal shock and to oxidation of metal diborides-SiC ceramics for aerospace application, J. Am. Ceram. Soc. 90 (2007) 1130–1138.
[5] J.W. Zimmermann, G.E. Hilmas, W.G. Fahrenholtz, Thermal shock resistance of ZrB_2 and ZrB_2–30% SiC, Mater. Chem. Phys. 112 (2008) 140–145.
[6] G.J. Zhang, Z.Y. Deng, N. Kondo, J.F. Yang, T. Ohji, Reactive hot pressing of ZrB_2–SiC composites, J. Am. Ceram. Soc. 83 (2000) 2330–2332.
[7] A.L. Chamberlain, W.G. Fahrenholtz, G.E. Hilmas, D.T. Ellerby, High-strength zirconium diboride-based ceramics, J. Am. Ceram. Soc. 87 (2004) 1170–1172.
[8] J.K. Kurihara, T. Tomimatsu, Y.F. Liu, S.Q. Guo, Y. Kagawa, Mode I fracture toughness of SiC particle-dispersed ZrB_2 matrix composite measured using DCDC specimen, Ceram. Int. 36 (2010) 381–384.
[9] Y.G. Wang, M.A. Zhu, L.F. Cheng, L.T. Zhang, Fabrication of SiC_w reinforced ZrB_2-based ceramics, Ceram. Int. 36 (2010) 1787–1790.
[10] D. Sciti, S. Guicciardi, A. Bellosi, G. Pezzotti, Properties of a pressureless-sintered ZrB_2–$MoSi_2$ ceramic composite, J. Am. Ceram. Soc. 89 (2006) 2320–2322.
[11] M.M. Opeka, I.G. Talmy, J.A. Zaykoski, Oxidation-based materials selection for 2000 °C plus hypersonic aerosurfaces: theoretical considerations and historical experience, J. Mater. Sci. 39 (2004) 5887–5904.
[12] M. Gasch, D. Ellerby, E. Irby, S. Beckman, M. Gusman, S. Johnson, Processing, properties and arc jet oxidation of hafnium diboride/silicon carbide ultra high temperature ceramics, J. Mater. Sci. 39 (2004) 5925–5937.
[13] D. Sciti, M. Brach, A. Bellosi, Oxidation behavior of a pressureless sintered ZrB_2–$MoSi_2$ ceramic composite, J. Mater. Res. 20 (2005) 922–930.
[14] A. Bellosi, F. Monteverde, D. Sciti, Fast densification of ultra-high-temperature ceramics by spark plasma sintering, Int. J. Appl. Ceram. Technol. 3 (2006) 32–40.
[15] Y.L. Jeng, E.J. Lavernia, Processing of molybdenum disilicide, J. Mater. Sci. 29 (1994) 2557–2571.
[16] Z. Yao, J. Stiglich, T.S. Sudarshan, Molybdenum silicide based materials and their properties, J. Mater. Eng. Perform. 8 (1999) 291–304.
[17] D. Sciti, F. Monteverde, S. Guicciardi, G. Pezzotti, A. Bellosi, Microstructure and mechanical properties of ZrB_2–$MoSi_2$ ceramic composites produced by different sintering techniques, Mater. Sci. Eng. A 434 (2006) 303–309.
[18] W.W. Wu, Z. Wang, G.J. Zhang, Y.M. Kan, P.L. Wang, ZrB_2–$MoSi_2$ composites toughened by elongated ZrB2 grains via reactive hot pressing, Scripta Mater. 61 (2009) 316–319.
[19] S.Q. Guo, T. Mizuguchi, M. Ikegami, Y. Kagawa, Oxidation behavior of ZrB_2–$MoSi_2$–SiC composites in air at 1500 °C, Ceram. Int. 37 (2011) 585–591.

[20] L. Silvestroni, D. Sciti, Effects of $MoSi_2$ additions on the properties of Hf- and Zr–B_2 composites produced by pressureless sintering, Scripta Mater. 57 (2007) 165–168.
[21] D. Sciti, M. Nygren, Spark plasma sintering of ultra refractory compounds, J. Mater. Sci. 43 (2008) 6414–6421.
[22] H.T. Liu, J. Zou, D.W. Ni, W.W. Wu, Y.M. Kan, G.J. Zhang, Textured and platelet-reinforced ZrB_2-based ultra-high-temperature ceramics, Scripta Mater. 65 (2011) 37–40.
[23] F. Monteverde, Progress in the fabrication of ultra-high-temperature ceramics: in situ synthesis, microstructure and properties of a reactive hot-pressed HfB_2–SiC composite, Compos. Sci. Technol. 65 (2005) 1869–1879.
[24] S.K. Mishra, S.K. Das, V. Sherbacov, Fabrication of Al_2O_3–ZrB_2 in situ composite by SHS dynamic compaction: a novel approach, Compos. Sci. Technol. 67 (2007) 2447–2453.
[25] J.J. Moore, H.J. Feng, Combustion synthesis of advanced materials: 1. Reaction parameters, Prog. Mater. Sci. 39 (1995) 243–273.
[26] G.J. Zhang, M. Ando, J.F. Yang, T. Ohji, S. Kanzaki, Boron carbide and nitride as reactants for in situ synthesis of boride-containing ceramic composites, J. Eur. Ceram. Soc. 24 (2004) 171–178.
[27] G.J. Zhang, X.M. Yue, Z.Z. Jin, Preparation and microstructure of TiB_2–TiC–SiC platelet-reinforced ceramics by reactive hot-pressing, J. Eur. Ceram. Soc. 16 (1996) 1145–1148.
[28] G.J. Zhang, Z.Z. Jin, X.M. Yur, A multilevel ceramic composite of TiB_2–$Ti_{0.9}W_{0.1}C$–SiC prepared by in situ reactive hot pressing, Mater. Lett. 28 (1996) 1–5.
[29] G.J. Zhang, Z.Z. Jin, X.M. Yue, TiB_2–Ti(C,N)–SiC composites prepared by reactive hot pressing, J. Mater. Sci. Lett. 15 (1996) 26–28.
[30] S. Ran, O. Van der Biest, J. Vleugels, In situ platelet-toughened TiB_2–SiC composites prepared by reactive pulsed electric current sintering, Scripta Mater. 64 (2011) 1145–1148.
[31] L. Silvestroni, H.J. Kleebe, S. Lauterbach, M. Muller, D. Sciti, Transmission electron microscopy on Zr- and Hf-borides with $MoSi_2$ addition: densification mechanisms, J. Mater. Res. 25 (2010) 828–834.
[32] J. Zou, S.K. Sun, G.J. Zhang, Y.M. Kan, P.L. Wang, T. Ohji, Chemical reactions, anisotropic grain growth and sintering mechanisms of self-reinforced ZrB_2–SiC doped with WC, J. Am. Ceram. Soc. 94 (2011) 1575–1583.
[33] X.W. Zhu, Y. Sakka, Textured silicon nitride: processing and anisotropic properties, Sci. Technol. Adv. Mater. 9 (2008) 033001.
[34] D.W. Ni, G.J. Zhang, Y.M. Kan, Y. Sakka, Highly textured ZrB_2-based ultrahigh temperature ceramics via strong magnetic field alignment, Scripta Mater. 60 (2009) 615–618.
[35] N.L. Okamoto, M. Kusakari, K. Tanaka, H. Inui, M. Yamaguchi, S. Otani, Temperature dependence of thermal expansion and elastic constants of single crystals of ZrB_2 and the suitability of ZrB_2 as a substrate for GaN film, J. Appl. Phys. 93 (2003) 88–93.
[36] J.J. Petrovic, M.I. Pena, I.E. Reimanis, M.S. Sandlin, S.D. Conzone, H.H. Kung, D.P. Butt, Mechanical behavior of $MoSi_2$ reinforced-Si_3N_4 matrix composites, J. Am. Ceram. Soc. 80 (1997) 3070–3076.
[37] G. Wen, S.B. Li, B.S. Zhang, Z.X. Guo, Reaction synthesis of TiB_2–TiC composites with enhanced toughness, Acta Mater. 49 (2001) 1463–1470.